Weak ferromagnetism in perovskite oxides

J.-S. Zhou,* L. G. Marshall,† Z.-Y. Li, X. Li, and J.-M. He
Materials Science and Engineering Program, Mechanical Engineering, The University of Texas at Austin, Austin, Texas 78712, USA

(Received 13 May 2020; revised 7 July 2020; accepted 30 August 2020; published 16 September 2020)

Weak ferromagnetism has been widely found in antiferromagnetic systems, including the technically important orthorhombic perovskites $R\mathrm{FeO_3}$ (R = rare earth) owing to spin canting associated with crystal symmetry. Antisymmetric exchange interaction (AEI) and single-ion anisotropy (SIA) are the essential mechanisms responsible for the development of noncollinear structures in antiferromagnetic systems. AEI and SIA share the same structural restriction to facilitate the spin canting. While both AEI and SIA originate from the spin-orbit coupling effect, they have sharply different dependences on the local structure. Consideration of the structural dependence of a canted spin motivates us to revisit the orthoferrite family. The spin canting along the c axis measured on precisely oriented crystals increases monotonically from $\mathrm{LaFeO_3}$ to $\mathrm{LuFeO_3}$. Based on Moriya's model, AEI is sensitive to the octahedral-site distortion in the perovskite structure. However, the site distortion does not exhibit a monotonic change with the rare-earth substitution. Instead, a linear relationship has been found in both the octahedral rotation and the spin canting angle versus the rare-earth ionic radius, which indicates that SIA plays a significant role leading the spin canting in orthoferrites.

DOI: 10.1103/PhysRevB.102.104420

I. INTRODUCTION

Weak ferromagnetism as an intrinsic property in antiferromagnets such as hematite was first recognized by Dzyaloshinskii in 1958 [1]. The magnetic anisotropy of the crystal competes with the superexchange interaction to give rise to the noncollinear spin structures. At the same time, Bozorth rationalized the weak ferromagnetism in the *Pbnm* perovskite $R\mathrm{FeO_3}$ based on the crystal field and the structural symmetry [2]. Moriya has shown a treatment of the microscopic mechanism of weak ferromagnetism by taking into account the spin-orbit coupling (SOC) in the superexchange interaction [3]. The antisymmetric exchange interaction in the formula $\boldsymbol{D}\cdot(\boldsymbol{S}_1\times\boldsymbol{S}_2)$ has been widely cited as Dzyaloshinskii-Moriya interaction (DMI) appearing in Hamiltonians to account for the spin canting. In addition, as stressed by Moriya [3], the DMI can exist only where the crystal symmetry is sufficiently low. A recent measurement of weak ferromagnetism in $\mathrm{FeBO_3}$ can be well accounted for by the DMI model [4]. Although both the DMI and the crystal field effect or the single-ion anisotropy (SIA) share the same requirement on the crystal symmetry and give a comparable magnitude of spin canting, in most cases spin canting has been attributed to the DMI. In the perovskite $\mathrm{BiFeO_3}$, both DMI and SIA terms have been included in a Hamiltonian to simulate a neutron inelastic scattering result [5]. The relevant studies on the orthoferrites were basically provided by Treves and his co-workers in the 1960s [6–10]. Within these works, the torque measurement has been widely cited as the most convincing evidence for the DMI.

The torque measurement gives the difference of the magnetic susceptibilities along the major crystallographic axes. The sensitivity of the torque measurement is significantly higher than the magnetic susceptibility measurement (10^{-3} emu) at Bell Laboratory in the 1960s [6]. The sign of the C_{ijk} tensor (in the free energy) has been determined from the torque measurement and compared with the outcomes from the SIA and the DMI models. The possibility of applying SIA to account for the spin canting has been ruled out since the authors incorrectly assigned the preferred crystallographic direction (PCD) to orthoferrites. The most troublesome problem in their conclusion comes from the term H_b, the anisotropy constant in the antisymmetric exchange model. Fitting the torque results to the DMI model yields a H_b corresponding to a more distorted $\mathrm{FeO_6}$ octahedron in $\mathrm{LaFeO_3}$ than that in $\mathrm{YFeO_3}$. The fitting results contradict the refinement results of x-ray diffraction and the results of the Mössbauer study on the orthoferrites [10–13]. Since the results of the spin canting moment for the entire family of orthoferrites reported in the literature [6,7,10] are inconsistent, this important parameter has not been used to distinguish the DMI versus the SIA. We are motivated to precisely measure the spin canting moment in the $R\mathrm{FeO_3}$ series and rationalize results with the DMI and the SIA models.

II. SAMPLE PREPARATION AND CHARACTERIZATION

$R\mathrm{FeO_3}$ single crystals were grown with the floating-zone method in an infrared-heating image furnace (NEC SC-M35HD). Crystal growth proceeded in a flow of air with a growing speed of 10 mm/h. The starting ceramic rods of $R\mathrm{FeO_3}$ were the product of a solid-state reaction between

*jszhou@mail.utexas.edu
†Present address: VitalFlo Inc., 310 S. Harrington St., Raleigh, NC 27603.

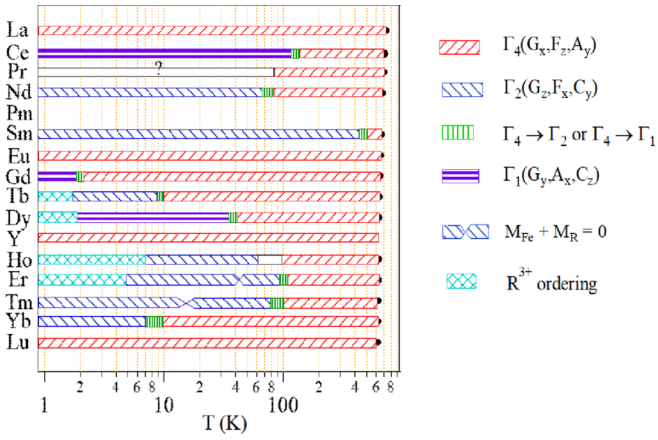

FIG. 1. The magnetic phase diagram of orthoferrites.

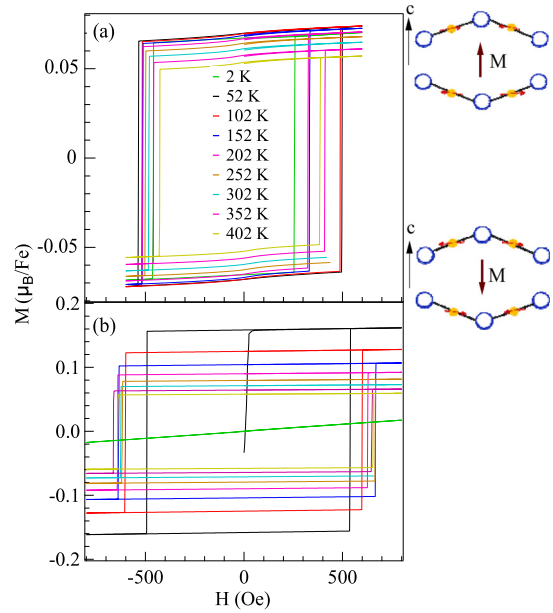

FIG. 2. The *M*-*H* loops at different temperatures for (a) $LuFeO_3$ and (b) $YbFeO_3$. The plot on the side of (a) shows schematically the magnetization switching along the *c* axis. Instead of changing the magnetic domain boundary, the sharp magnetization switching is made possible by simply flipping spins by 180°. Blue circles denote oxygen, solid yellow circles Fe^{3+}, and red arrows spins at Fe^{3+}.

R_2O_3 (Alfa Aesar, 99.9%+) and Fe_2O_3 (Alfa Aesar, 99.998%) in a 1:1 molar ratio. The phase purity was confirmed by powder x-ray diffraction. Laue back reflection was used to check the crystal quality and to orient the crystals along the three principal axes with an error less than 1°. Magnetization measurements were carried out in a superconducting quantum interference device (SQUID) magnetometer and a Vibration Sample Magnetometer (VSM) in Physical Property Measurement System (PPMS); both setups are from Quantum Design.

III. RESULTS AND DISCUSSION

Bertaut [14] has shown that the *Pbnm* perovskite structure can accommodate antiferromagnetic spin structures described by the four irreducible representations: $\Gamma_1(A_x, G_y, C_z)$, $\Gamma_2(F_x, C_y, G_z)$, $\Gamma_3(C_x, F_y, A_z)$, $\Gamma_4(G_x, A_y, F_z)$. The phase diagram of orthoferrites [15,16] in Fig. 1 indicates all but $SmFeO_3$ adopt Γ_4 at room temperature. The noncollinear spin structure in orthoferrites can be determined by neutron diffraction [17,18]. The canted moment can also be measured accurately from the magnetization loop at $H = 0$ on a precisely oriented, high-quality crystal. The component of the total moment, $M_z(0)$ [$M_x(0)$ for $SmFeO_3$] can be extracted by fitting $M_z(T)$ or [$M_x(T)$ for $SmFeO_3$] to the Brillouin function $B_{J=5/2}(T)$. Typical magnetization data of $M_z(H)$ at different temperatures in the range $2\,\mathrm{K} < T < 400\,\mathrm{K}$ for some $R\mathrm{FeO_3}$ crystals are shown in Fig. 2. The magnetic structure of those with a magnetic rare earth becomes complicated by the rare-earth magnetic moment and a possible exchange coupling with Fe^{3+}. Depending on the anisotropy of the rare earth, the rare-earth moment can be parallel or antiparallel to the internal field generated by the Fe-O array. The exchange interaction between R^{3+} and Fe^{3+} also leads to the transformation from the spin structure of Γ_4 to Γ_2 or Γ_1 depending on R [19] as temperature decreases, as is shown in Fig. 1. Similar to the formula used by Cooke *et al.* [20] when they described the total magnetization of $GdCrO_3$, the magnetization $M(T)$ of $R\mathrm{FeO_3}$ can be expressed as

$$M(T) = M_{\mathrm{Fe}} + C_R(H_I + H_a)/(T + \theta), \tag{1}$$

where M_{Fe} is the canting moment from the magnetically ordered FeO_3 array, which should follow the Brillouin function; C_R is the Curie constant for the magnetic rare earth R; H_I is the internal magnetic field at the R^{3+} site; and H_a is the applied magnetic field. Since $M(T)$ is the magnetization obtained at $H_a = 0$ and H_I should be proportional to M_{Fe}, we can simplify the fitting formula to

$$M(T) = B_J(T)[1 \pm a/T]. \tag{2}$$

The sign of the second term in the equation depends on the magnetic anisotropy on R^{3+}. A Curie law (instead of a Curie-Weiss law) is used for simplicity since the exchange interaction between rare earths is relatively small. Figure 3 shows the $M_z(T)$ [$M_x(T)$ for $SmFeO_3$] data of $R\mathrm{FeO_3}$ crystals. The quality of fitting the data to the formula in Eq. (2) is good. Although all the magnetization measurements were performed below 400 K, T_{N} of $R\mathrm{FeO_3}$ from the fitting is comparable to that in the literature [10], which further supports the validity of the procedure. For R = Nd, Sm, Gd, Er, the rare-earth moment is antiparallel to the internal field from the canted spin, whereas it is parallel for R = Dy, Tm, Yb. A spin canting angle $\theta = 0.53°$ at 0 K is obtained for $LaFeO_3$ given $5\,\mu_{\mathrm{B}}$ on Fe^{3+}, which is nearly identical to the canting angle derived by neutron scattering [21]. The reduced spin canting angle $\theta_r = (\theta - \theta_{\mathrm{La}})/\theta_{\mathrm{La}}$ versus the rare-earth radius (IR) is shown in Fig. 4. The data points can be separated into two groups, one for the nonmagnetic R = La,Y, Lu, and another for the magnetic rare earths. A line can be drawn to connect three points of θ_r for R = La, Y, Lu. While scattered over a quite large range of θ_r for those with magnetic R in $R\mathrm{FeO_3}$, it is interesting to note that θ_r's for the rare earths with an odd number of $4f$ electrons are generally higher than those with an even number of $4f$ electrons and the θ_r (for odd $4f$) increases monotonically as the IR decreases. A great scattering of the

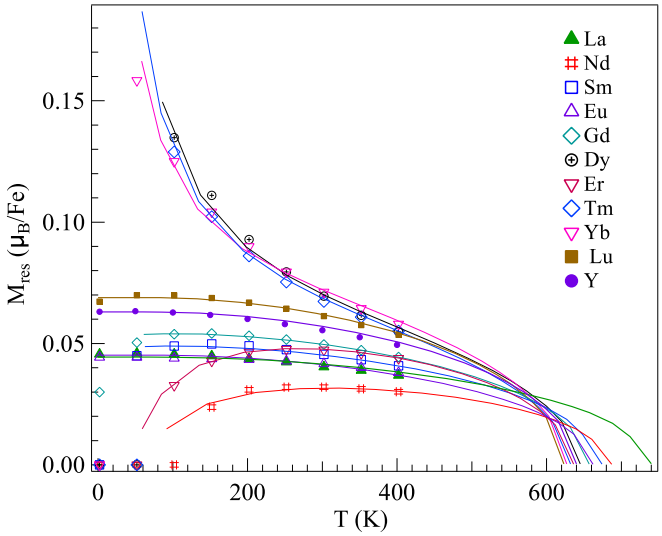

FIG. 3. Temperature dependence of the residual moment M_{res} obtained from the $M(H)$ loops at $H_a = 0$ for RFeO$_3$; lines are the fitting results to the Brillouin function for the diamagnetic rare earths or the function of Eq. (1) in the text for the magnetic rare earths. The abrupt drop of the canted moment at low temperatures for the RFeO$_3$ with R = Nd, Dy, Er, and Tm is due to the spin reorientation at T_{SR}. Below T_{SR}, the formula of Eq. (2) is invalid for the fitting in these cases.

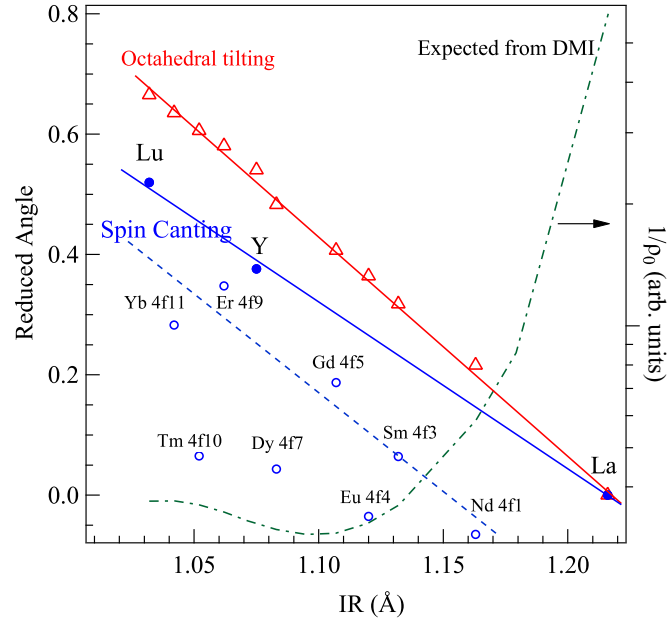

FIG. 4. Reduced spin canting angle θ_r and the octahedral-site rotation angle β_r versus IR of orthoferrite RFeO$_3$; solid lines are drawn as a guide to the eyes. The dot-dash line is a schematic drawing for the spin canting angle based on the change of the local crystal structure. The solid blue circles denote the reduced angle for the RFeO$_3$ with nonmagnetic rare earth. The hollow blue circles are for those RFeO$_3$ with magnetic rare earths; the dashed line is a guide to the eyes, which is drawn within the data points for the RFeO$_3$ with the rare earths having odd numbers of $4f$ electrons. The data of the reduced angle in the figure represent the change of the canting moment of RFeO$_3$ relative to that in LaFeO$_3$. On the other hand, the DMI theory predicts that the canting moment is proportional to the correction of the Landé factor in the crystal field. The correction is inversely proportional to the bond length splitting. Therefore, the data in the figure show the relative change of the canted moment from the experiment and the prediction of the DMI model as a function of the rare-earth radius.

data for those with magnetic rare earths may be due to an oversimplified fitting formula of Eq. (2) and the spin structural transitions at low temperatures as indicated in Fig. 1. The observation of a linear increase of the spin canting angle θ_r in the RFeO$_3$ (R = La, Y, Lu) as the IR decreases may offer an important clue for identifying the weak ferromagnetism in the perovskites. The data of the canted moment in RFeO$_3$ from this work and from the literature are listed in Table I. A systematic change of the canted moment found in the RFeO$_3$ with nonmagnetic rare earths observed in this work is missed in the data from the literature.

The rare-earth substitution in RFeO$_3$ changes the geometric tolerance factor, which leads to a different degree of the orthorhombic distortion. It is important to examine how the spin canting in either the DMI or the SIA models is related to the crystal structure. A key point in Moriya's theory is that the spin canting angle depends on the correction on the Landé g factor due to the SOC effect, i.e., $\tan\theta \sim D/2J \sim \Delta g/g$, $\Delta g = g - 2$ [3,22,23]. It is important to know whether and how Δg depends on detailed changes of crystal structure from LaFeO$_3$ to LuFeO$_3$. The g factor for orthoferrites available

TABLE I. The saturation moment along the canting direction (or the canted angle) in RFeO$_3$. The reduced canted angle is defined as $\theta_r = (\theta - \theta_{La})/\theta_{La}$.

	La	Pr	Nd	Sm	Eu	Gd	Tb	Dy	Y	Ho	Er	Tm	Yb	Lu
[a]$M(0)$, μ_B	**0.046**		0.043	0.049	0.044	0.054		0.048	**0.063**		0.062	0.049	0.059	**0.07**
[a]Canted angle (deg)	**0.53**		0.49	0.56	0.51	0.63		0.55	**0.72**		0.71	0.56	0.68	**0.80**
[a]Reduced angle	**0**		–0.065	0.064	–0.035	0.19		0.043	**0.38**		0.35	0.065	0.28	**0.52**
[b]Canted angle (deg)	**0.52**	0.49	0.49	0.47	0.46	0.56	0.44	0.46	**0.51**	0.47	0.46	0.46	0.51	**0.61**
[c]$M(0)$ (μ_B)	**0.047**			0.041	0.04	0.049	0.039	0.04	**0.045**	0.041	0.041	0.04	0.045	**0.054**
[d]$M(0)$ (emu/g)	**1.2**								**1.0**					**1.0**

[a]This work.
[b]From Ref. [10].
[c]From Ref. [7].
[d]From Ref. [6].

in the literature is not complete for the entire series. The difference of the g factor between $YFeO_3$ and $LuFeO_3$ is smaller than the measurement uncertainty [24]. We turn to the explicit expression of the g tensor given by White [25]. In the effective spin Hamiltonian,

$$H_{\text{eff}} = \sum_{\varepsilon,\tau} \left(\mu_B g_{\varepsilon,\tau} H_\epsilon S_\tau - \lambda^2 \Lambda_{\varepsilon,\tau} S_\varepsilon S_\tau - \mu_B^2 \Lambda_{\varepsilon,\tau} H_\varepsilon H_\tau\right),$$

$$\Lambda_{\varepsilon,\tau} = \sum_{\rho'} \frac{|\langle\rho|L_\varepsilon|\rho'\rangle\langle\rho'|L_\tau|\rho\rangle}{E_{\rho'} - E_\rho}, \tag{3}$$

and $g_{\varepsilon\tau} = 2(\delta_{\varepsilon\tau} - \lambda\Lambda_{\varepsilon\tau})$, $\varepsilon, \tau = x, y, z$. $|\rho\rangle$ represents the $2L+1$-fold orbital part of the wave functions; $|\rho\rangle$s for the five electrons in free-ion Fe^{3+} reduce to a single S-wave function ($L = 0$), so that $\Lambda_{\varepsilon\tau}$ vanishes in the free-ion model. For Fe^{3+} in the cubic crystal field, the wave function of the $2L+1$-fold orbital part in free ion becomes $x^2 - y^2$, $3z^2 - r^2$, xy, yz, zx. Since Fe-O bonds in the FeO_6 octahedra split into long, medium, and short bonds, the wave function of the ground state should be a mixture of $x^2 - y^2$ and $3z^2 - r^2$. A finite $\Lambda_{\varepsilon\tau}$, an eigenvalue for the orbital operators L_x, L_y, and L_z (in the coordination of the primary perovskite cell), is obtained for the Fe^{3+} ion in the octahedron having the smallest bond length splitting. Depending on the evolution of the local distortion from La to Lu in orthoferrites, we expect to see a corresponding profile of $\lambda\Lambda_{\varepsilon\tau}$ and therefore a spin canting angle.

Whereas the octahedral-site rotation in the orthoferrites is inversely proportional to IR, octahedra in the *Pbnm* perovskites have normally been treated to be rigid, which means that the local coordination of FeO_6 octahedra, therefore $\Lambda_{\varepsilon\tau}$, is independent of IR. If this assumption is true, the spin canting angle should have no change between different members for the entire family. However, rigid octahedra cannot be linked together into a three-dimensional (3D) system with octahedral-site rotations around fixed axes [26]. Experiments [12,27] indeed revealed the evolution of bond length splitting as a function of IR in Fig. 5. The bond length splitting, which can be described by orthorhombic vibration modes Q_2 and Q_3, shows a maximum in the middle IR of the family $RFeO_3$ [28]. Since the magnitude $\rho = (Q_2^2 + Q_3^2)^{1/2}$ reflects the bond length splitting in an octahedron, the expectation value of the orbital angular moment operators, $\Lambda_{\varepsilon\tau}$, must be inversely proportional to ρ. The largest spin canting angle is expected to occur at the side of $R =$ La, then the second largest canting angle at the side of $R =$ Lu; the minimum of canting should occur at the middle of IR (near $R =$ Gd), as indicated schematically by the curve $1/\rho$ in Fig. 4. The derived profile of spin canting angle from the structure does not match the observation. The profile of local deformation is also highly consistent with the quadruple splitting from the Mössbauer effect mapping over $RFeO_3$, which is a local probe for detecting structural distortions [10].

While widely cited, the treatment of the superexchange interaction as the spin-orbit interaction is included by Moriya is oversimplified. In a review paper about the weak ferromagnetism in $3d$ insulators, Moskvin [29] gave the most complete description of the DMI; specifically, the structure factor was included in the formula of DMI for the *Pbnm* perovskites. Unfortunately, the strength of the Dzyaloshinskii vector needs

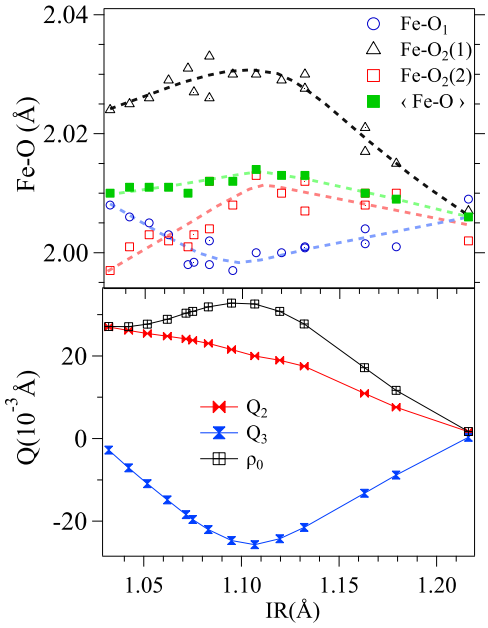

FIG. 5. Upper panel: Three Fe-O bond lengths versus IR in orthoferrites; dashed lines are guides to the eyes. Lower panel: the orthorhombic vibration modes $Q_2 = (l_x - l_y)$ and $Q_3 = (2l_z - l_x - l_y)/\sqrt{3}$, where l_x denotes the Fe-O bond length, and the magnitude of local bond length splitting $\rho = (Q_2^2 + Q_3^2)^{1/2}$ versus IR. The structural data are after Refs. [11,27].

to be determined experimentally. As the DMI model cannot account for the profile of spin canting angle in orthoferrites, we turn to SIA in these perovskites.

The easy axis of the magnetic moment in a magnetically ordered phase is determined by the magnetic anisotropy which is generated by a combination of SIA and the crystal symmetry [30]. The possible easy axes in magnetic perovskites have been found roughly along the direction of the M-O bond (in type-C antiferromagnetism (AF) or the Γ_2 structure of type G AF), to the middle of the edge of the octahedron from M (common), and to the center of the triangular face of the octahedron from M (in the rhombohedral phase only) [31]. The second term in Eq. (3) of the spin Hamiltonian is the energy of the single-ion anisotropy. It is again related directly to the second-order perturbation term $\Lambda_{\varepsilon\tau}$. For the structure having an axial symmetry $\Lambda_{xx} = \Lambda_{yy} = \Lambda_\perp$, $\Lambda_{zz} = \Lambda_\parallel$, for example, the SIA term can be simplified as $D[S_z^2 - (1/3)S(S+1)]$, where $D = \lambda^2(\Lambda_\parallel - \Lambda_\perp)$. This expression points out explicitly that the easy axis should be along the highest symmetric axis of the octahedron in the perovskite structure. In the orthoferrites, the Fe-O bonds in the FeO_6 octahedron split into long, medium, and short bonds with the long and short bonds in the basal plane and the medium bond on the c axis as shown in Fig. 6. Therefore, the axis with the highest symmetry cannot be along a Fe-O bond direction, but along the a or b axis of the orthorhombic cell. In addition, an easy axis along the Fe-O bonding direction would have a large magnetostatic energy cost as spin arrows will face each other collinearly in the type-G antiferromagnetic structure. It is our essential assumption that the PCD for the magnetization in the type-G

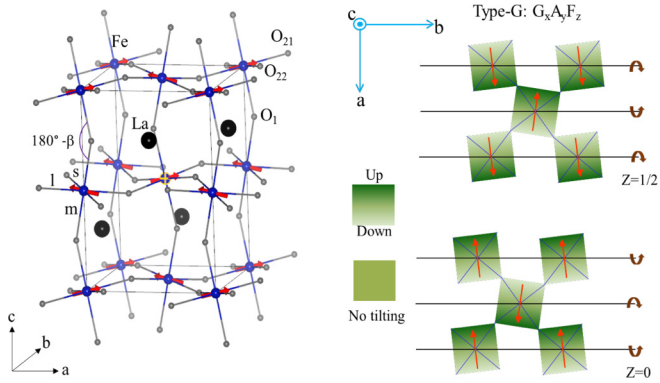

FIG. 6. Schematic structural model and the spin structure of orthoferrites. Left: the orthorhombic perovskite structure of $LaFeO_3$; Right: Octahedron in *a*-*b* plane projected along the *c* axis. The preferred crystallographic direction is represented by red arrows inside the octahedra.

AF perovskite is along the line through Fe to the middle of an edge of an octahedron as illustrated in Fig. 6.

The tilting system $a^-a^-c^+$ of the *Pbnm* space group can be decomposed into two submodes of $a^-a^-c^0$ and $a^0a^0c^+$. The octahedral-site rotation in the major rotation mode $a^-a^-c^0$ (around the *b* axis of the *Pbnm* cell, the rotation axis in Fig. 6) causes the PCD tilting from the *ab* plane. The tilting angle β can be estimated to be $180^\circ - \angle(\text{Fe-O}_1\text{-Fe})^\circ$ in Fig. 6. For type-*G* AF ordering G_x, the SIA effect from the PCD tilting creates the spin canting on the same direction along the *c* axis, F_z, as illustrated in Fig. 6. Moreover, the out-of-phase rotation of the octahedron around the *c* axis and therefore the PCD creates the spin tilting in *ab* planes toward the *b* axis and $-b$ axis alternately along the *c* axis, which adds the A_y component to the spin structure. Therefore, the *Pbnm* perovskite structure has all the ingredients to facilitate the noncollinear spin structure $\Gamma_4(G_x, A_y, F_z)$ found by neutron diffraction [21]. The coupling to the PCD is the primary driving force to induce the spin canting. The tilting angle β of the PCD because of the octahedral-site tilting of the $a^-a^-c^0$ mode increases monotonically as the IR decreases from the structural study. The reduced tilting angle $\beta_r = (\beta - \beta_{\text{La}})/\beta_{\text{La}}$ is superimposed in the plot of Fig. 4. The spin canting is closely correlated to the PCD. The spin canting driven by the SIA effect competes with the much stronger superexchange interaction leading to collinear spin orderings, which explains the small angle between β_r(IR) and θ_r(IR).

IV. CONCLUSION

While a sufficiently lower crystal symmetry is required for spin canting to be present in both the DMI and the SIA models, the underlying mechanisms are different. To determine which model is appropriate in the case of $R\text{FeO}_3$, we directly measured the spin canting angle in single crystals and observed a monotonic change of the spin canting in the series. In the DMI model, the magnitude of spin canting depends on how the local structural distortion alters the Landé *g* factor from $g = 2$ in the DMI model. However, the analysis of $\Delta g = g - 2$ based on the evolution of local structure in orthoferrites $R\text{FeO}_3$ fails to account for the monotonic change of the spin canting observed herein. By contrast, the change of spin canting has been found to be correlated with the change of the Fe-O-Fe bond angle, which is consistent with SIA. This observation suggests that the single-ion anisotropy effect is responsible for the spin canting in the type-*G* antiferromagnets orthoferrites.

ACKNOWLEDGMENTS

This work was supported by NSF (Grant No. DMREF 1729588). The authors are grateful to John B. Goodenough for his continuous interest, insightful discussion, and support.

[1] I. Dzyaloshinsky, J. Phys. Chem. Solids **4**, 241 (1958).
[2] R. M. Bozorth, Phys. Rev. Lett. **1**, 362 (1958).
[3] T. Moriya, Phys. Rev. **120**, 91 (1960).
[4] V. E. Dmitrienko, E. N. Ovchinnikova, S. P. Collins, G. Nisbet, G. Beutier, Y. O. Kvashnin, V. V. Mazurenko, A. I. Lichtenstein, and M. I. Katsnelson, Nat. Phys. **10**, 202 (2014).
[5] J. Jeong, M. D. Le, P. Bourges, S. Petit, S. Furukawa, S.-A. Kim, S. Lee, S.-W. Cheong, and J.-G. Park, Phys. Rev. Lett. **113**, 107202 (2014).
[6] D. Treves, Phys. Rev. **125**, 1843 (1962).
[7] D. Treves, J. Appl. Phys. **36**, 1033 (1965).
[8] D. Treves and S. Alexander, J. Appl. Phys. **33**, 1133 (1962).
[9] D. Treves, M. Eibschut, and P. Coppens, Phys. Lett. **18**, 216 (1965).
[10] M. Eibschutz, S. Shtrikman, and D. Treves, Phys. Rev. **156**, 562 (1967).
[11] M. Marezio, J. P. Remeika, and P. D. Dernier, Acta Crystallogr., Sect. B: Struct. Sci., Cryst. Eng. Mater. **26**, 2008 (1970).
[12] M. Marezio, J. P. Remeika, and P. D. Dernier, Acta Crystallogr. B: Struct. Sci., Cryst. Eng. Mater. **26**, 300 (1970).
[13] P. Coppens and P. Eibschutz, Acta Crystallogr. **19**, 524 (1965).
[14] E. F. Bertaut, in *Magnetism*, Vol. III, edited by G. T. Rado and H. Sull (Academic Press, New York, 1963), pp. 149.
[15] Y. Endoh, K. Kakurai, A. K. Katori, M. S. Seehra, G. Srinivasan, and H. P. J. Wijn, in *Magnetic Properties of Non-Metallic Inorganic Compounds Based on Transition Elements: Perovskites II, Oxides with Corundum, Ilmenite and Amorphous Structures, Landolt-Börnstein, New Series*, edited by H. P. J. Wijn (Springer-Verlag, New York, 1994), Vol. 27f3, p. 101.
[16] K. Enke, J. Fleischhauer, W. Gunber, P. Hansen, S. Nomura, W. Tolksdorf, G. Winkler, and U. Wolfmeier, in *Numerical Data and Functional Relationships in Science and Technology, Landolt-Börnstein*, edited by K.-H. Hellwege and A. M. Hellwege (Springer-Verlag, New York, 1978), Vol. 12, p. 451.
[17] T. Peterlinneumaier and E. Steichele, J. Magn. Magn. Mater. **59**, 351 (1986).
[18] V. P. Plakhty, Y. P. Chernenkov, M. N. Bedrizova, and J. Schweizer, in *Neutron Scattering —1981*, AIP Conf. Proc. No. 89 (AIP, Melville, NY, 1982), p. 330.

[19] T. Yamaguchi, J. Phys. Chem. Solids **35**, 479 (1974).
[20] A. H. Cooke, D. M. Martin, and M. R. Wells, J. Phys. C: Solid State Phys. **7**, 3133 (1974).
[21] K. Park, H. Sim, J. C. Leiner, Y. Yoshida, J. Jeong, S. Yano, J. Gardner, P. Bourges, M. Klicpera, V. Sechovsky, M. Boehm, and J. Park, J. Phys.: Condens. Matter **30**, 235802 (2018).
[22] T. Moriya, Phys. Rev. Lett. **4**, 228 (1960).
[23] T. Moriya, *Magnetism* (Academic Press, New York, 1963).
[24] G. Gorodetsky, J. Phys. Chem. Solids **30**, 1745 (1969).
[25] R. M. White, *Quantum Theory of Magnetism*, 2nd corrected and updated ed. (Springer-Verlag, New York, 1983).
[26] M. O'Keeffe and B. G. Hyde, Acta Crystallogr., Sect. B: Struct. Sci., Cryst. Eng. Mater. **33**, 3802 (1977).
[27] M. Marezio and P. D. Dernier, Mater. Res. Bull. **6**, 23 (1971).
[28] J. S. Zhou and J. B. Goodenough, Phys. Rev. B **77**, 132104 (2008).
[29] A. Moskvin, Condens: Matter **4**, 84 (2019).
[30] J. M. D. Coey, *Magnetism and Magnetic Materials* (Cambridge University Press, Cambridge, 2010).
[31] J. S. Zhou, J. A. Alonso, A. Muonz, M. T. Fernandez-Diaz, and J. B. Goodenough, Phys. Rev. Lett. **106**, 057201 (2011).